Hybrid fiber grating cavity for multi-parametric sensing

Domenico Paladino[1], Giuseppe Quero[1], Christophe Caucheteur[2], Patrice Mégret[2], and Andrea Cusano[1,*]

[1]*Optoelectronic Division-Engineering Department, University of Sannio, C.so Garibaldi 107, 82100 Benevento, Italy*
[2]*Electromagnetism and Telecommunication Unit, Faculté Polytechnique de Mons, Bd Dolez 31, 7000 Mons, Belgium*
**a.cusano@unisannio.it*

Abstract: We propose an all-fiber hybrid cavity involving two unbalanced uniform fiber Bragg gratings (FBGs) written at both sides of a tilted FBG (TFBG) to form an all-fiber interferometer. This configuration provides a wavelength gated reflection signal with interference fringes depending on the cavity features modulated by spectral dips associated to the wavelength dependent optical losses due to cladding mode coupling occurring along the TFBG. Such a robust structure preserves the advantages of uniform FBGs in terms of interrogation methods and allows the possibility of simultaneous physical and chemical sensing.

OCIS codes: (050.2230) Fabry-Perot; (050.2770) Gratings; (060.2340) Fiber optics components; (060.2370) Fiber optics sensors; (230.1480) Bragg reflectors.

References and links

1. K. O. Hill, B. Malo, F. Bilodeau, D. C. Johnson, and J. Albert, "Bragg gratings fabricated in monomode photosensitive optical fiber by UV exposure through a phase mask," Appl. Phys. Lett. **62**(10), 1035–1037 (1993).
2. A. Othonos and K. Kalli, *Fiber Bragg Gratings Fundamentals and Applications in Telecomminications and Sensing* (Artech House, Boston, 1999).
3. R. Kashyap, *Fiber Bragg Gratings* (Academic Press, San Diego, 1999).
4. L. Zhang, W. Zhang, and I. Bennion, "In-fiber grating optic sensors," in *Fiber Optics Sensors*, F. T. S. Yu and S. Yin, eds. (Dekker, New York, 2002), Chap. 4.
5. A. Mendez, "Fiber Bragg grating sensors: A market overview," Proc. SPIE **6619**, paper 661905 (2007).
6. G. Meltz, S. J. Hewlett, and J. D. Love, "Fiber grating evanescent wave sensors," Proc. SPIE **2836**, 342–350 (1996).
7. K. Usbeck, W. Ecke, A. Andreev, V. Hagemann, R. Mueller, and R. Willsch, "Distributed optochemical sensor network using evanescent field interaction in fiber Bragg gratings," Proc. SPIE **3483**, 90–94 (1998).
8. A. Asseh, S. Sandgren, H. Ahlfeldt, B. Sahlgren, R. Stubbe, and G. Edwall, "Fiber optical Bragg grating refractometer," Fiber Integr. Opt. **17**, 51–62 (1998).
9. A. Iadicicco, A. Cusano, A. Cutolo, R. Bernini, and M. Giordano, "Thinned fiber Bragg gratings as high sensitivity refractive index sensor," IEEE Photon. Technol. Lett. **16**(4), 1149–1151 (2004).
10. A. Iadicicco, S. Campopiano, A. Cutolo, M. Giordano, and A. Cusano, "Nonuniform thinned fiber Bragg gratings for simultaneous refractive index and temperature measurements," IEEE Photon. Technol. Lett. **17**(7), 1495–1497 (2005).
11. A. Iadicicco, A. Cusano, S. Campopiano, A. Cutolo, and M. Giordano, "Microstructured fiber Bragg gratings: Analysis and fabrication," Electron. Lett. **41**(8), 466–468 (2005).
12. A. Iadicicco, A. Cusano, S. Campopiano, A. Cutolo, and M. Giordano, "Refractive index sensor based on micro-structured fiber Bragg grating," IEEE Photon. Technol. Lett. **17**(6), 1250–1252 (2005).
13. A. Iadicicco, S. Campopiano, D. Paladino, A. Cutolo, and A. Cusano, "Micro-structured fiber Bragg gratings: optimization of the fabrication process," Opt. Express **15**(23), 15011–15021 (2007), http://www.opticsinfobase.org/abstract.cfm?URI=oe-15-23-15011.
14. D. Paladino, A. Iadicicco, S. Campopiano, and A. Cusano, "Not-lithographic fabrication of micro-structured fiber Bragg gratings evanescent wave sensors," Opt. Express **17**(2), 1042–1054 (2009), http://www.opticsinfobase.org/oe/abstract.cfm?uri=oe-17-2-1042.
15. K. Zhou, Y. Lai, X. Chen, K. Sugden, L. Zhang, and I. Bennion, "A refractometer based on a micro-slot in a fiber Bragg grating formed by chemically assisted femtosecond laser processing," Opt. Express **15**(24), 15848–15853 (2007), http://www.opticsinfobase.org/oe/abstract.cfm?URI=oe-15-24-15848.
16. J. C. Knight, T. A. Birks, P. St. J. Russell, and D. M. Atkin, "All-silica single-mode optical fiber with photonic crystal cladding," Opt. Lett. **21**(19), 1547–1549 (1996).
17. B. J. Eggleton, P. S. Westbrook, R. S. Windeler, S. Spälter, and T. A. Strasser, "Grating resonances in air-silica microstructured optical fibers," Opt. Lett. **24**(21), 1460–1462 (1999).

#124953 - $15.00 USD Received 2 Mar 2010; revised 16 Apr 2010; accepted 21 Apr 2010; published 5 May 2010

18. N. Groothoff, I. Canning, E. Buckley, K. Lyttikainen, and J. Zagari, "Bragg gratings in air-silica structured fibers," Opt. Lett. **28**(4), 233–235 (2003).
19. L. B. Fu, G. D. Marshall, J. A. Bolger, P. Steinvurzel, E. C. Mägi, M. J. Withford, and B. J. Eggleton, "Femtosecond laser writing Bragg gratings in pure silica photonic crystal fibres," Electron. Lett. **41**(11), 638–640 (2005).
20. S. J. Mihailov, D. Grobnic, H. Ding, C. W. Smelser, and J. Broeng, "Femtosecond IR laser fabrication of Bragg gratings in photonic crystal fibers and tapers," IEEE Photon. Technol. Lett. **18**(17), 1837–1839 (2006).
21. M. C. P.han Huy, G. Laffont, Y. Frignac, V. Dewynter-Marty, P. Ferdinand, P. Roy, J.-M. Blondy, D. Pagnoux, W. Blanc, and B. Dussardier, "Fibre Bragg grating photowriting in microstructured optical fibres for refractive index measurement," Meas. Sci. Technol. **17**(5), 992–997 (2006).
22. M. C. P. Huy, G. Laffont, V. Dewynter, P. Ferdinand, P. Roy, J.-L. Auguste, D. Pagnoux, W. Blanc, and B. Dussardier, "Three-hole microstructured optical fiber for efficient fiber Bragg grating refractometer," Opt. Lett. **32**(16), 2390–2392 (2007).
23. A. Cusano, D. Paladino, and A. Iadicicco, "Micro-structured fiber Bragg gratings," J. Lightwave Technol. **27**(11), 1663–1697 (2009).
24. G. Laffont and P. Ferdinand, "Tilted short-period fibre-Bragg-grating-induced coupling to cladding modes for accurate refractometry," Meas. Sci. Technol. **12**(7), 765–770 (2001).
25. C. Chen and J. Albert, "Strain-optic coefficients of individual cladding modes of a singlemode fibre: theory and experiment," Electron. Lett. **42**(18), 1027–1028 (2006).
26. S. Baek, Y. Jeong, and B. Lee, "Characteristics of short-period blazed fiber Bragg gratings for use as macro-bending sensors," Appl. Opt. **41**(4), 631–636 (2002).
27. T. Erdogan and J. E. Sipe, "Tilted fiber phase gratings," J. Opt. Soc. Am. A **13**(2), 296–313 (1996).
28. C. Caucheteur and P. Mégret, "Demodulation technique for weakly tilted fiber Bragg grating refractometer," IEEE Photon. Technol. Lett. **17**(12), 2703–2705 (2005).
29. C. Caucheteur, D. Paladino, P. Pilla, A. Cutolo, S. Campopiano, M. Giordano, A. Cusano, and P. Mégret, "External refractive index sensitivity of weakly tilted fiber Bragg gratings with different coating thicknesses," IEEE Sens. J. **8**(7), 1330–1336 (2008).
30. C.-F. Chan, C. Chen, A. Jafari, A. Laronche, D. J. Thomson, and J. Albert, "Optical fiber refractometer using narrowband cladding-mode resonance shifts," Appl. Opt. **46,** 1142–1149 (2007).
31. T. Guo, C. Chen, A. Laronche, and J. Albert, "Power referenced and temperature-calibrated optical fiber refractometer," IEEE Photon. Technol. Lett. **20**(8), 635–637 (2008).
32. C. Caucheteur, M. Wuilpart, C. Chen, P. Mégret, and J. Albert, "Quasi-distributed refractometer using tilted Bragg gratings and time domain reflectometry," Opt. Express **16**(22), 17882–17890 (2008), http://www.opticsinfobase.org/abstract.cfm?URI=oe-16-22-17882.
33. C. Caucheteur, S. Bette, C. Chen, M. Wuilpart, P. Mégret, and J. Albert, "Tilted fiber Bragg grating refractometer using polarization-dependent loss measurements," IEEE Photon. Technol. Lett. **20**(24), 2153–2155 (2008).
34. S. Maguis, G. Laffont, P. Ferdinand, B. Carbonnier, K. Kham, T. Mekhalif, and M.-C. Millot, "Biofunctionalized tilted Fiber Bragg Gratings for label-free immunosensing," Opt. Express **16**(23), 19049–19062 (2008), http://www.opticsinfobase.org/oe/abstract.cfm?URI=oe-16-23-19049.
35. C. Caucheteur, P. Mégret, and A. Cusano, "Tilted Bragg grating multipoint sensor based on wavelength-gated cladding-modes coupling," Appl. Opt. **48**(20), 3915–3920 (2009).
36. P. Childs, A. C. L. Wong, I. Leung, G.-D. Peng, and Y. B. Liao, "An in-line in-fibre ring cavity sensor for localized multi-parameter sensing," Meas. Sci. Technol. **19**(6), 065302 (2008).
37. Y. Liu and K. S. Chiang, "Fiber-Bragg-grating cavity sensor interrogated with a self-seeded Fabry-Pérot laser diode," IEEE Photon. Technol. Lett. **18**(20), 2153–2155 (2006).
38. J. M. Vaughan, *The Fabry-Perot Interforometer: History, Theory, Practice and Applications* (Taylor & Francis Group, New York, 1989).
39. A. Cusano, A. Iadicicco, D. Paladino, S. Campopiano, and A. Cutolo, "Photonic band-gap engineering in UV fiber gratings by the arc discharge technique," Opt. Express **16**(20), 15332–15342 (2008), http://www.opticsinfobase.org/oe/abstract.cfm?uri=oe-16-20-15332.

1. Introduction

In 1993, the demonstration of the phase mask technique greatly simplified the manufacture of fiber Bragg gratings (FBGs) [1]. The prospect of manufacturing high performance gratings at low cost was critical to the large scale implementation of this technology, especially for sensing applications. As matter of fact, over the last fifteen years, FBGs have been utilized as optical sensors to measure a wide range of physical parameters including temperature and strain [2–5].

Along a uniform FBG, the propagating core mode couples with the contra-propagating one, allowing the final device to be used as a wavelength selective mirror. The basic interrogation mechanism relies on monitoring the resonant wavelength in the reflected signal by the grating in order to detect changes in external parameters. Their flexibility of design to be used as single point or multi-point sensing arrays and their relative low cost, make FBGs

#124953 - $15.00 USD Received 2 Mar 2010; revised 16 Apr 2010; accepted 21 Apr 2010; published 5 May 2010

ideal devices to be adopted for a multitude of different sensing applications. However, since the light coupling takes place between well-bound core modes that are screened from the influence of the surrounding refractive index (SRI) by the cladding, uniform FBGs are intrinsically not useful in chemical sensing applications. To make them SRI sensitive, hosting optical fiber must be structured in some way to allow the interaction of the guided light with the surroundings.

One approach relies on structuring the cladding layer of optical fibers in which FBGs are successively or previously manufactured to allow evanescent wave interaction. Interesting solutions involving D-shaped optical fibers [6], planar side polishing [7], uniformly thinned FBGs [8,9], non-uniform thinned FBGs [10], micro-structured FBGs [11–14], and micro-slotted FBGs [15] have been proposed. In all of these cases, the structural integrity of the pristine optical fiber is compromised and, as direct consequence, weakening of the final device should be faced up.

On the other side, after the publication by Knight et al. in 1996 [16], the research interest in microstructured optical fibers (MOFs) dramatically grew up. MOFs are optical fibers structurally including transverse microstructures extending parallelly to the fiber propagation axis. Differently from conventional optical fibers, MOFs do not need appropriate post-processing treatments to reach SRI sensitization. The interesting feature of MOFs, in fact, is the intrinsic interaction between the guided optical electromagnetic field and the medium inserted into the holes. Even if important issues such as high levels of scattered light and rotationally variant symmetry had to be taken into account during grating writing, the first FBG within MOFs was successfully demonstrated in 1999 [17]. Successively, starting from the results already achieved on conventional optical fibers, several other successful writing operations have been reported [18–20]. Finally, also FBG writing within MOFs has now reached a good level of maturity.

In the last years, Phan Huy et al. exploited the refractive index sensitivity of FBGs written within different MOFs geometry [21,22]. Such sensitivity, in fact, can be enhanced by a convenient design of the MOF hosting the grating. However appropriate managing of the liquid flow inside the fiber channels has to be guaranteed for an efficient sensor head design. In addition, one of the main MOFs limitations is that they are still much more expansive technological platforms if compared to conventional optical fibers.

Detailed information about all the abovementioned configurations can be found in a recent review paper [23].

In contrast to microstructured FBGs, an alternative approach towards SRI sensitization relies on the use of tailored grating features to obtain the adequate sensitivity to the external medium as in the case of tilted FBGs (TFBGs). In TFBGs, the core refractive index modulation pattern characterizing short-period fiber gratings is blazed by an angle θ with respect to the fiber axis. This asymmetry enables and enhances the coupling of the guided core mode with circularly and non-circularly symmetric contra-propagating cladding modes, reducing, in turn, the coupling efficiency to the contra-propagating core mode (the Bragg peak strength). As direct consequence, TFBGs provide a direct tool for in-fiber refractometers due to the intrinsic sensitivity of the cladding modes on the SRI. In practice, the cladding layer acts as an interface with the external medium making TFBGs intrinsically SRI sensitive [24].

A single TFBG provides temperature insensitive SRI measurements [24], as well as axial strain measurements [25] or bending measurements [26]. Due to the peculiar coupling mechanism – if the angle θ is sufficiently low (typically less than 12°) – both a core mode resonance and several cladding mode resonances appear simultaneously in the TFBG transmission spectrum [27]. This has several advantages: the cladding mode resonances are sensitive to the external perturbations (SRI, bending, etc.) while the core mode resonance, i.e. the Bragg resonance, is only sensitive to temperature and mechanical strain. It has been observed that the temperature sensitivity of the cladding modes is similar to that of the core mode so that the effect of temperature can be removed from a simultaneous monitoring of the cladding and core modes [25].

#124953 - $15.00 USD Received 2 Mar 2010; revised 16 Apr 2010; accepted 21 Apr 2010; published 5 May 2010

To demodulate the transmission spectrum of a TFBG subjected to an external perturbation, two typical techniques have been originally proposed. The first one, based on the global monitoring of the area delimited in the spectrum by the cladding modes, is particularly suited for SRI measurements [24,28]. In addition, a proper modification of the demodulation technique based on the monitoring of spectra partitions depending on the cladding mode order provides a valuable tool for sensitivity tailoring and re-configurability [29]. On the other hand, an alternative methodology relies on local monitoring of selected cladding mode resonance shifts: in this case, calculating their displacement with respect to the Bragg wavelength could allow temperature insensitive measurements [25,30]. To correctly operate, these techniques require transmitted spectrum measurement on a wavelength range of a few tens of nanometers, severely complicating the demodulation technique of such sensing elements.

Recently particular attention has been devoted to investigate novel TFBGs interrogation methods such as transmitted power monitoring [31], optical time domain reflectometry [32], polarization-dependent loss measurements [33], and predominant frequency monitoring of the transmission spectrum Fourier transform [34]. However since uniform FBGs still represent a better assessed technology, also their interrogation techniques are simpler and more cost effective.

On this line of argument, it would be extremely useful to opportunely combine uniform FBGs and TFBGs in a single in-fiber structure to obtain multi-parametric simultaneous measurements maintaining the advantages of FBGs interrogation. A first attempt to obtain

A first solution has been proposed by the authors in Ref [35]. In that case a hybrid configuration involving a TFBG followed by a uniform FBG working in reflection mode – allowing also multipoint sensing – was demonstrated and experimentally validated for refractive-index sensing purposes. However, the recent work by Childs et al. on TFBGs demonstrated the potentialities of an in-line in-fiber ring cavity configuration for refractometric purposes [36]. To exploit the advantages of a cavity structure contemporarily maintaining a working principle similar to the one reported in Ref [35], in this work the design, the realization, and the experimental characterization of an all-fiber hybrid cavity for quasi-distributed sensing purposes is demonstrated. The cavity is made by an unbalanced interferometer composed of two uniform FBGs in the middle of which a TFBG is inscribed. Because of its intrinsic nature, the investigated hybrid cavity preserves both uniform FBGs and TFBGs spectral sensitivity. The proposed configuration offer simple multi-parametric measurements working in reflection mode with a wavelength gated signal. In particular, experimental results demonstrate that such a structure can be usefully exploited to simultaneously measure multiple parameters (SRI, bending, temperature, and strain) by simple measurements based on both wavelength shift and normalized reflectance changes.

An all-fiber three grating elements cavity structure was also proposed as a SRI sensor by Liu and Chiang in 2006 [37]. In that case the lateral mirrors were two chirped FBGs and between them a long-period fiber grating was interposed.

2. All-fiber hybrid cavity: design, realization and characterization

In this section, a detailed description of the interferometric cavity is reported.

2.1 Design and realization

The principle of operation is extremely simple and it is based on the structure schematically reported in Fig. 1: the all-fiber device is composed by two unbalanced uniform FBGs and an interposed TFBG with a small tilt angle (weakly TFBG).

#124953 - $15.00 USD Received 2 Mar 2010; revised 16 Apr 2010; accepted 21 Apr 2010; published 5 May 2010

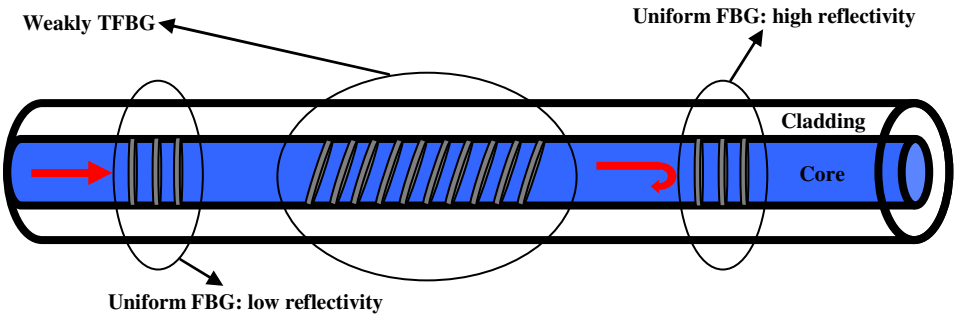

Fig. 1. Schematic diagram of the proposed all-fiber hybrid interferometric cavity (not in scale).

The lateral FBGs are designed to be accorded at approximately the same wavelength. This way they work as the mirrors of an in-fiber interferometric cavity. Note that at least one of the gratings reflectivities has to be lower that 100% in order to allow the inteferometric operation. On the other hand, since the aim of the authors is to interrogate such a structure in reflection from the non-strong FBG side, the other reflector has to be a high reflectivity grating in order to obtain the maximum useful signal to the interrogation unit. Finally, the presence of the TFBG within the cavity is aimed to modulate the propagating light through cladding modes coupling. In particular, the TFBG has to be designed in order to allow spectral overlapping between selected cladding mode resonances and mirrors spectrum.

All the grating elements were manufactured into hydrogen loaded Corning® single-mode optical fiber by means of a frequency-doubled Argon ion laser at 244 nm and a phase mask. For TFBG inscription, the uniform phase mask was mounted on a rotating stage in order to apply a tilt in the plane perpendicular to the incident laser beam. As matter of fact, well assessed technological facilities readily allow the fabrication of all the three fiber gratings constituting the all-fiber cavity.

From here on, experimental results concerning two different cavity structures will be reported: the cavities geometrical features and the involved gratings parameters are resumed in Table 1. The left and right uniform FBGs are referred to the scheme of Fig. 1.

Table 1. Resume of the investigated cavities features.

	Uniform FBGs Length	Left FBG Maximum Reflectivity	Right FBG Maximum Reflectivity	Uniform FBGs Central Wavelength	TFBG Length	TFBG Tilt Angle	Total Cavity Length
1st Cavity	0.5 mm	~30%	~100%	~1577.7 nm	4 mm	4°	~25 mm
2nd Cavity	0.5 mm	~30%	~100%	~1574.7 nm	3 mm	2°	~25 mm

2.2 Characterization

To monitor the cavity spectral response in reflection a simple optoelectronic setup was used. It comprised a broadband super-luminescent diode operating at 1550 nm with 40 nm full width half maximum bandwidth, a 3 dB coupler, and an optical spectrum analyzer (Ando AQ6317C) with a resolution of 10 pm.

The spectral evolution of the 2° all-fiber hybrid interferometric cavity during its realization process is presented in Fig. 2, together with a schematic diagram of the structure obtained after each step. The fiber structure after the writing of the lateral uniform FBGs is reported on the right hand side in Fig. 2(a). The presence of two selective mirrors accorded at the same resonant wavelength generates a Fabry-Pérot interferometric cavity. Due to this phenomenon, the resultant reflected spectrum (from the low reflective FBG side) is the one reported on the left hand side in Fig. 2(a). As observable, the reported spectral response is analogous to the typical reflected spectrum from a single uniform FBG, but presents superimposed periodical interference fringes due to the Fabry-Pérot effect occurring along the

#124953 - $15.00 USD Received 2 Mar 2010; revised 16 Apr 2010; accepted 21 Apr 2010; published 5 May 2010

cavity. The spectral separation between such fringes is approximately 35-40 pm, confirming a cavity length of about 25 mm [38].

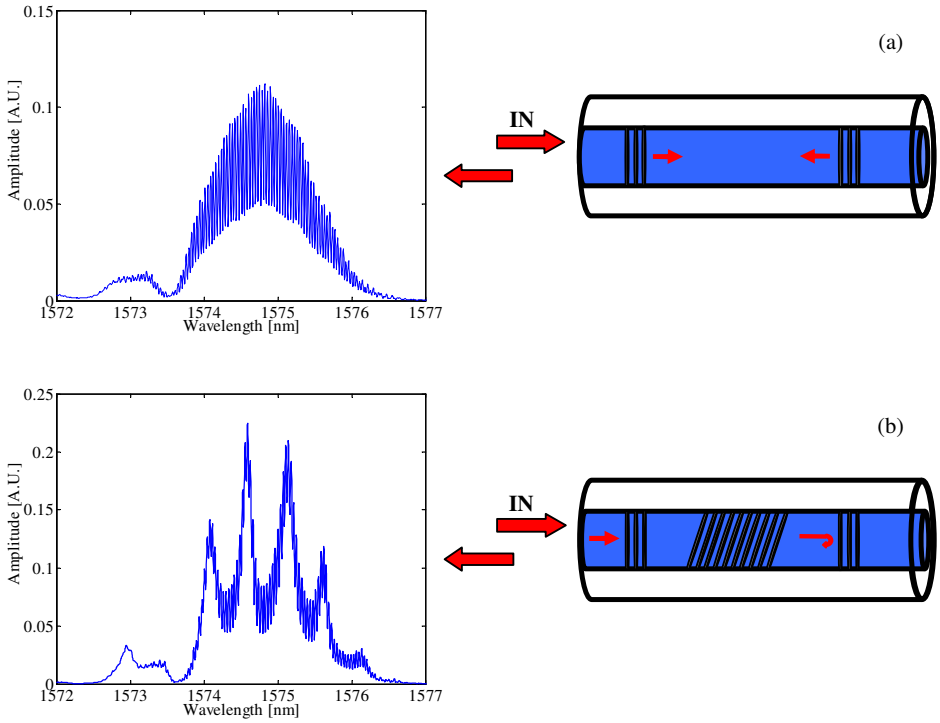

Fig. 2. Realization of the 2° all-fiber hybrid cavity: schematic diagram (not in scale) and reflected spectrum (a) after only uniform FBGs writing and (b) after adding the TFBG.

The last grating element to be written was the TFBG. After the TFBG inscription, the complete realization is accomplished as reported in the schematic diagram on the right hand side in Fig. 2(b). Also in this case, the experimental reflected spectrum is reported on the left hand side of the same figure. Now the wavelength gated signal reflected by the cavity formed by the two uniform FBGs is further modulated by the attenuation bands due to the cladding modes resonances of the TFBG overlapping with the mirrors spectra.

It is important to highlight that also the Bragg resonance of the weakly TFBG is present in the cavity reflected spectrum, but it is far from the cavity spectra.

As regards the device functionality, the so realized hybrid interferometric cavity is able to preserve the versatility of uniform FBGs with respect to measurements in reflection for strain and temperature sensing applications, adding also finer scale spectral features due to the presence of the attenuation bands of the TFBG, as well as to the interference fringes linked to the Fabry-Pérot effect occurring along the cavity. In addition, compared to a single TFBG, the structure preserves the spectral sensitivities to external parameters such as SRI and bending, but strongly reduces the useful signal bandwidth.

3. Experimental validation of the hybrid cavity spectral sensitivity

To evaluate the effective sensitivity of the proposed device for multi-parametric sensing applications, an experimental analysis has been carried out in terms of temperature, strain, SRI, and bending characterization.

3.1 Temperature and strain characterization

For the temperature characterization, a simple experimental setup based on the use of Peltier cells capable to control the local temperature along the cavity with a resolution of ± 0.1°C was

#124953 - $15.00 USD Received 2 Mar 2010; revised 16 Apr 2010; accepted 21 Apr 2010; published 5 May 2010

adopted [39]. It is important to note that the entire cavity structure was in close contact with the heating element, allowing uniform temperature changes all along the fiber structure.

Figure 3 shows the 4° TFBG hybrid cavity spectral response for different local temperatures, varying in the range 20°-70°C. As observable, temperature increase leads only to a red shift of the reflected spectrum, analogously to what happens for uniform FBGs. As direct consequence, usual uniform FBGs interrogation techniques based on wavelength shift monitoring of wavelength gated signals could be adopted to detect temperature changes.

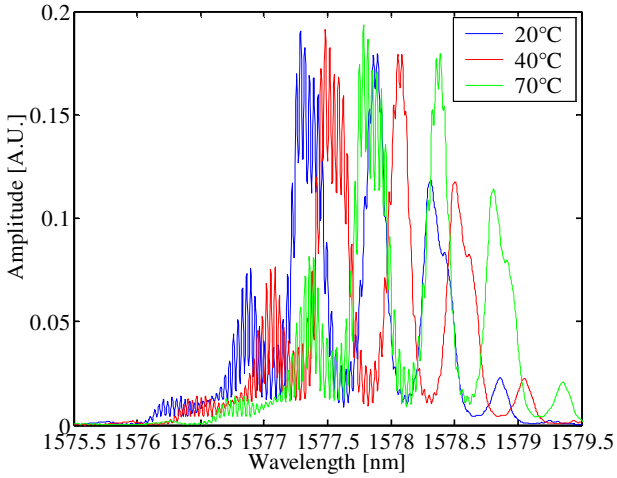

Fig. 3. 4° TFBG hybrid cavity spectra for different temperatures ranging between 20 and 70°C.

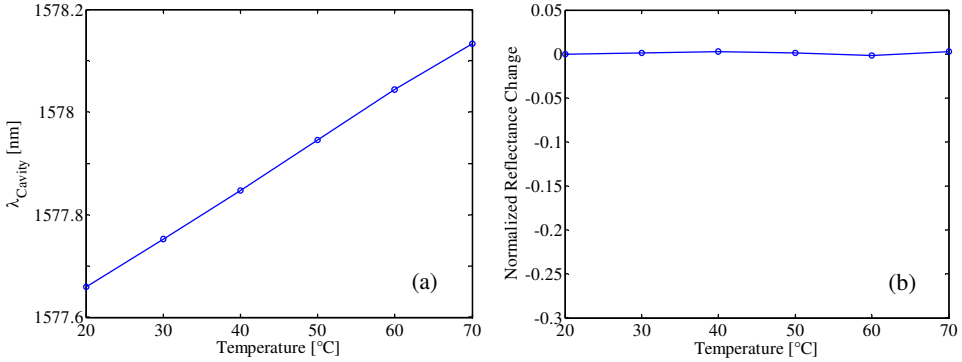

Fig. 4. 4° TFBG hybrid cavity characterization versus temperature (20-70°C): (a) Shifts of the central wavelength; (b) Normalized reflectance changes.

In particular, Fig. 4(a) shows the cavity central wavelength versus temperature. It has been estimated as the average value between the wavelengths corresponding to the edges of the whole wavelength gated signal reflected by the cavity, independently on the presence or the absence of the interference fringes due to the Fabry-Pérot effect. The diagram reveals an extremely linear behavior, with a sensitivity value of 9.5 pm/°C (a typical value for UV written uniform FBGs [39]). To be completely sure that temperature changes cause only a wavelength shift of the cavity spectral response, also the reflectance changes have been monitored. In particular, the total reflected power (P) from the wavelength gated signal by the hybrid cavity has been computed as function of temperature. Specifically, Fig. 4(b) shows the total reflectance changes during the temperature characterization, normalized to the total reflected power at 20°C – $(P-P_{20°C})/P_{20°C}$. Note how the cavity total reflectance shows a

#124953 - $15.00 USD Received 2 Mar 2010; revised 16 Apr 2010; accepted 21 Apr 2010; published 5 May 2010

constant behavior, confirming that the only spectral effect due to the temperature increase is a red shift of the reflected spectrum from the cavity.

Very similar results have been obtained during the strain characterization. In this case the cavity was stretched by fixing one end of the structure and applying different weights to the other termination [39].

Figure 5 shows the 4° TFBG hybrid cavity spectral response as the applied mass varies in the range 5.063-30.110 g. As observable, also for increasing strain state a red shift of the spectrum reflected back by the cavity has been registered.

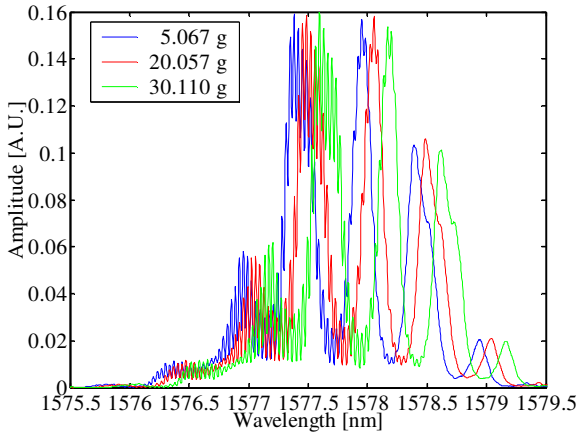

Fig. 5. 4° TFBG hybrid cavity spectra for different applied mass (meaning different longitudinal strain state along the cavity) ranging between 5.063 and 30.110 g.

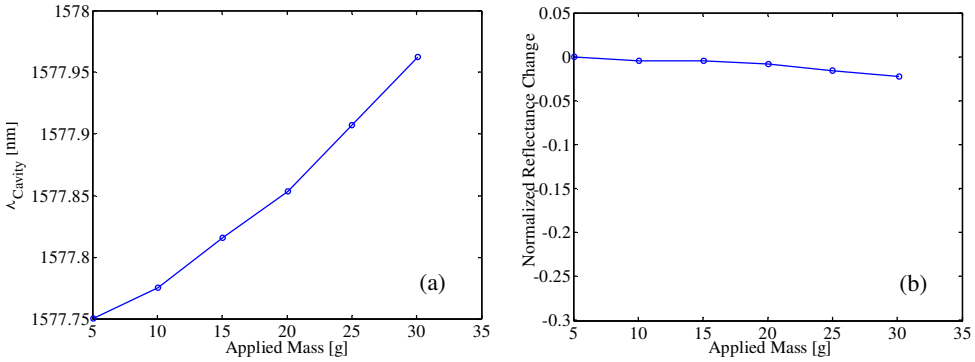

Fig. 6. 4° TFBG hybrid cavity characterization versus applied mass (5.063-30.110 g): (a) Shifts of the central wavelength; (b) Normalized reflectance changes.

Figure 6(a) shows the cavity central wavelength behavior during the strain characterization. In this case the variation is not perfectly linear with an average sensitivity of about 8.5 pm/g. Also this value is similar to that of UV written uniform FBGs [39]. The non-exact linearity is probably due to the slightly different elasto-optic coefficients associated to the core and cladding modes involved in the cavity spectral response. This leads to a different wavelength shift of the cladding modes bands and the mirror spectra. Figure 6(b) shows the total reflected power changes from the cavity versus the applied strain, normalized to the total reflectance as the applied mass was 5.063 g. As observable, a small normalized reflectance change of about 2% has been pointed out in the investigated range.

#124953 - $15.00 USD Received 2 Mar 2010; revised 16 Apr 2010; accepted 21 Apr 2010; published 5 May 2010

3.2 SRI and bending characterization

Due to the presence of the TFBG, the all-fiber cavity should be sensitive also to external parameters such as SRI and bending. SRI tests have been carried out by immersing the cavity in a series of glycerin-water solutions at different concentrations [14]. The test solutions were characterized by means of a commercial Abbe refractometer with resolution of 10^{-4}. Figure 7 shows the spectral response of the 4° TFBG hybrid cavity for different SRIs in the range 1.4332-1.4699.

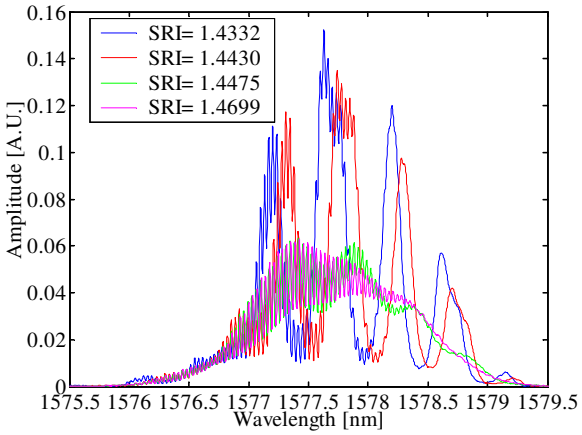

Fig. 7. 4° TFBG hybrid cavity spectra for different SRIs ranging between 1.4332 and 1.4699.

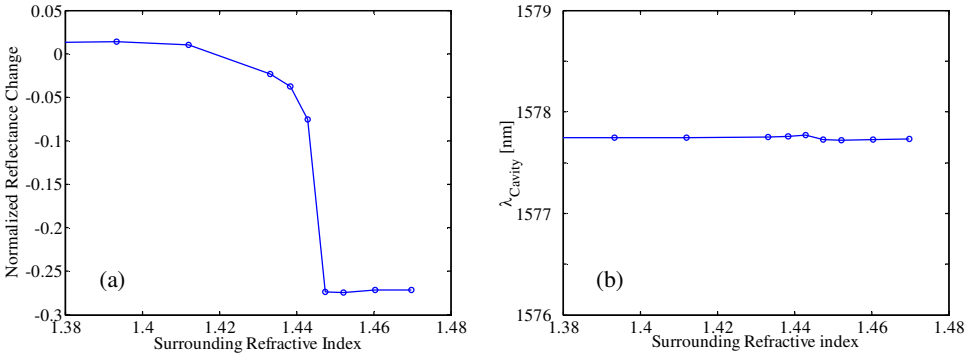

Fig. 8. 4° TFBG hybrid cavity characterization versus SRI: (a) Normalized reflectance changes; (b) Shifts of the central wavelength.

As well known from TFBGs theory [24,28], as the SRI increases the cladding mode resonances red shift due to the increase in the mode effective indices. In addition, approaching their cut-off condition, the attenuation bands progressively disappear starting from the ones at lower wavelengths (higher order cladding modes) and are gradually replaced by a broadband low level attenuation due to the coupling with a continuum of radiation modes. The same spectral effects can be observed for the cladding mode resonances involved in the cavity spectral response reported in Fig. 7. As direct consequence, strong normalized reflectance changes are observable versus the SRI. At the same time, since grating mirrors are SRI insensitive no wavelength shift of the cavity response occurs. This suggests a simple and fast interrogation technique based on total reflected power monitoring. Figure 8(a) shows the total reflectance changes – normalized to the total reflected power in air – for SRIs higher than 1.38. Note how the total reflected power by the cavity progressively decreases as the SRI

#124953 - $15.00 USD Received 2 Mar 2010; revised 16 Apr 2010; accepted 21 Apr 2010; published 5 May 2010

increases, up to reach a quasi-constant value when all the cladding mode dips involved in the reflected spectrum approach their cut-off condition. In particular, the total reflected power non-linearly decreases of approximately 28.1% as the SRI passes from 1.4120 to 1.4475. By supposing that 0.1% variations can be detected, a minimum SRI resolution of about 6×10^{-4} in the range 1.4120-1.4332 and a maximum resolution of about 2×10^{-5} in 1.4430-1.4475 have been obtained. In addition, note that the cut-off condition depends on the cladding mode order. As consequence, it is possible to design the cavity in order to select the required cladding modes an thus the SRI range where maximum sensitivity occurs.

Finally, Fig. 8(b) shows the behavior of the cavity central wavelength during the SRI characterization. As expected, in this case no wavelength shifts have been registered.

As last step, a bending characterization of the investigated structure has been carried out. To induce different bending states along the fiber segment containing the hybrid cavity, the fiber terminations were mounted onto two metallic bars as shown in Fig. 9. One of them was fixed, whereas the other one was made movable on a millimetric scale: by moving the metallic bar along the direction indicated by the black arrow in Fig. 9, it is possible to change the curvature radius (R) induced along the cavity structure. As matter of fact, the experiment starts with a maximum bending state induced along the cavity (R of about 8 mm) and successively the bending state is relaxed by moving the not-fixed metallic bar as previously described.

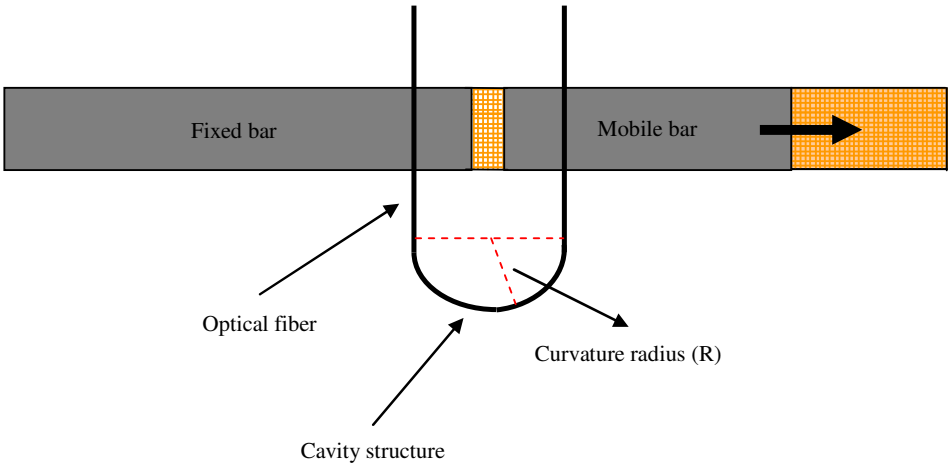

Fig. 9. Schematic diagram of the setup utilized for the bending characterization (not in scale).

Figure 10 shows the spectral response for different curvature radii ranging between 8 and 16 mm. Similarly to what happened during the SRI characterization, high bending state induces complete disappearance of the cladding mode dips from the reflected spectrum. In practice, small curvature radii force the cut-off condition of the cladding modes involved in the hybrid cavity spectral response. As direct consequence, the spectrum reflected by the cavity shows only interference fringes due to the Fabry-Pérot effect generated by the lateral mirrors (blue curve in Fig. 10: no effects due to the presence of the TFBG). On the contrary, by relaxing step-by-step the bending constraint – by increasing R – the free-bending reflected spectrum is progressively recovered. (red and green curves in Fig. 10: the presence of the cladding mode dips are clearly observable). This means that the cladding modes progressively get out of the cut-off condition, reaching their standard unperturbed propagation regime.

As direct consequence, total reflected power changes have been pointed out also during the bending characterization. In particular, Fig. 11(a) shows the total reflectance changes for curvature radii ranging between 8 and 24 mm – normalized to the case R = 24 mm, in which the free bending state is completely recovered. In particular, total reflectance decreases of almost 50% in the investigated curvature radii range. By supposing again that 0.1% variations

#124953 - $15.00 USD Received 2 Mar 2010; revised 16 Apr 2010; accepted 21 Apr 2010; published 5 May 2010

can be detected, a minimum R resolution of 56 μm in the range 20-22 mm and a maximum resolution of 7 μm in the range 8-10 mm can be obtained.

As reported in Fig. 11(b), also in this case no wavelength shift has been observed during the experimental characterization. This way, by acting on the TFBG spectral properties, SRI and bending state changes induce variations in the total reflected power by the hybrid cavity, without shifting its spectrum. Consequently, these parameters could be easily detected by intensity based measurements of the wavelength gated signal provided by the cavity.

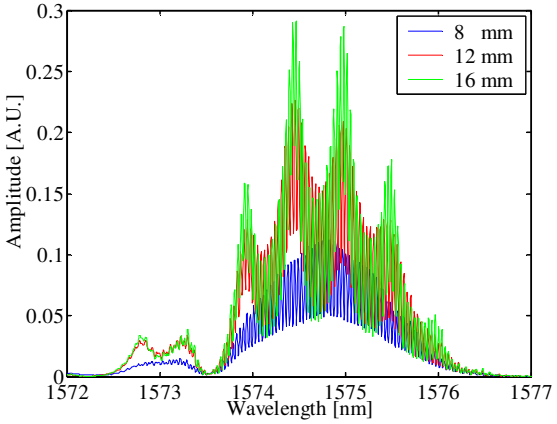

Fig. 10. 2° TFBG hybrid cavity spectra for different curvature radii varying from 8 to 16 mm.

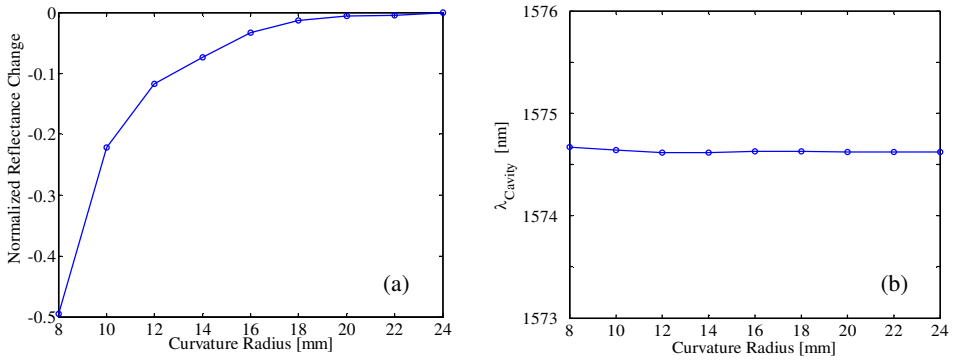

Fig. 11. 2° TFBG hybrid cavity characterization versus bending state: (a) Normalized reflectance changes; (b) Shifts of the central wavelength.

4. Discussion

Based on the reported results, two basic concepts rule the sensing measurements of the hybrid fiber grating cavity:

-external parameters such as temperature and strain – since core and cladding modes have very similar temperature sensitivities and not so dissimilar strain sensitivities – are able to induce mainly wavelength shifts in the signal reflected by the cavity;

-external parameters such as SRI and bending, instead, by significantly acting on the cladding modes coupling are able to modify the attenuation bands associated to the cladding modes resonances, leading to normalized reflectance changes.

Moreover, the setup utilized for the bending characterization suggests that the proposed hybrid cavity could be easily adopted as a sensing probe also in displacement sensing. As

#124953 - $15.00 USD Received 2 Mar 2010; revised 16 Apr 2010; accepted 21 Apr 2010; published 5 May 2010

described in Fig. 9, in fact, the cavity bending state has been changed by acting on the longitudinal position of the not fixed metallic bar. As direct consequence, since the longitudinal displacement of one of the fiber terminations corresponds to bending state changes along the cavity, with the same sensing mechanism both bending and displacement sensors could be configured.

In addition, an alternative approach can be also envisaged to measure SRI and bending by a proper elaboration of the spectral response. In fact, recently Maguis et al. exploited the apparent sinusoidal nature of the complex spectrum of a TFBG to determine SRI changes [34]. There is a continuum of frequencies within the Fourier transform of a TFBG transmission spectrum. When the SRI increases, the frequencies involved in the Fourier transform of the transmission spectrum gradually disappear. Since the lower the wavelength resonance is, the more the spectral distance between two consecutive dips increases, low wavelength resonances contribute to the low frequency component on the Fourier transform. As consequence, when the SRI changes, the predominant frequency of the Fourier transform of the TFBG spectral response can be considered for sensing.

Since SRI and bending mainly involve cladding mode coupling, the Fourier transform method has been evaluated as a valid alternative tool for the signal demodulation in case of SRI and bending sensing applications. In particular, Fig. 12 shows the fast Fourier transform (FFT) of some spectra from the 4° TFBG hybrid cavity acquired during the SRI characterization. The FFT of the reflected spectrum in air (black curve) is characterized by the presence of a predominant DC component due to the not null average value of the reflected spectrum and by low-frequency side-lobes associated to the cladding modes dips appearing within the reflected spectrum.

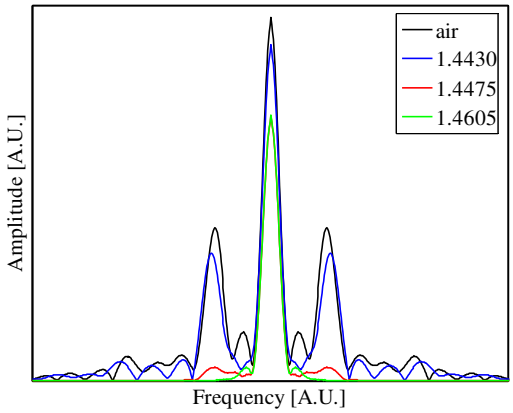

Fig. 12. FFT analysis of the 4° TFBG hybrid cavity spectral response for different SRIs.

As observable, as the SRI increases and approaches the cut-off condition of the cladding modes resonances, both spectral components progressively decrease in amplitude. Finally, when the cut-off condition has been completely reached, the DC component reaches a maximum amplitude diminution, whereas the low frequency side-lobes completely disappear from the FFT of the reflected spectrum (see the green curve). To completely understand the FFT behaviour, the DC component decrease in amplitude of about 28% as happens for the total reflected power during the SRI characterization (as described in the previous section). On the contrary, the low frequency side-lobes are subjected to a 100% reduction in amplitude. This means that side-lobes amplitude monitoring could be considered as an alternative observable parameter to measure SRI and bending state changes experienced by the cavity.

#124953 - $15.00 USD Received 2 Mar 2010; revised 16 Apr 2010; accepted 21 Apr 2010; published 5 May 2010

5. Conclusion

In this work, the design, realization, and experimental characterization of an all-fiber hybrid cavity structure for multi-parametric sensing purposes have been carried out. The proposed configuration provides a wavelength gated reflection signal modulated by interference fringes with a visibility dependent on the cladding mode coupling occurring along the TFBG.

Experimental results demonstrate simultaneous SRI, bending, temperature, and strain sensitivity. In particular, by wavelength shift monitoring, it is possible to detect temperature and strain changes while SRI and bending measurements can be obtained by simple intensity based detection. On this line of argument, an effective advantage of the hybrid cavity relies on the easy multiplexing capability of such structures.

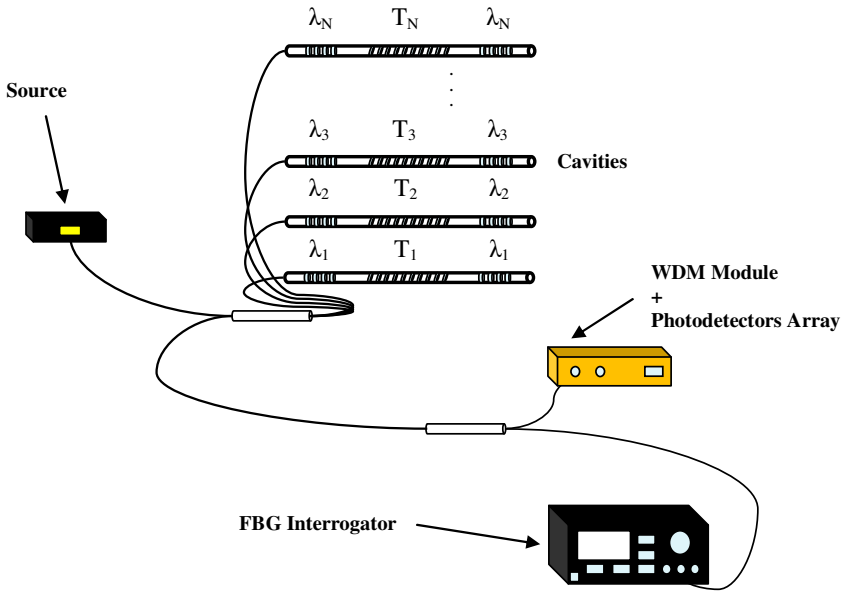

Fig. 13. Schematic diagram of a simple interrogation setup to interrogate several multiplexed all-fiber hybrid cavity structures for multi-parametric measurements (not in scale).

The narrow reflected signal bandwidth, in fact, could allow several hybrid fiber grating cavities to be multiplexed in a parallel configuration as reported in Fig. 13. As schematically reported in the figure, simple optoelectronic devices are needed to interrogate this kind of network. The reflected spectrum could be processed by means of standard interrogation equipments exploiting well assessed methods. In particular a standard interrogation unit for wavelength shift monitoring would be useful to detect temperature or strain changes, while a simple module able to detect changes in the total power reflected by each cavity would be useful to monitor SRI or bending state variations.

Moreover, since the detectable SRI range depends on the coupled cladding modes as described above, the sensors network could be also “complicated” by inscribing more than a single cavity on the same fiber by using a single TFBG and several uniform FBG couples, matched to different order cladding modes.

Before concluding the authors want to highlight the advantages of the sensing probe described in this paper with respect to other configurations previously reported in literature.

In comparison to the three elements cavity structure presented in 2006 [37], here, the adopted interrogation method relies on the well assessed approach based on wavelength shift monitoring and intensity based measurements, leading to cost effective, more compact and less complex sensor read out, also if more cavities are interrogated simultaneously. In addition, in despite of the lower complexity, the SRI resolution demonstrated in this paper, even if the structure is not optimized, is more than one order of magnitude higher than the one

#124953 - $15.00 USD Received 2 Mar 2010; revised 16 Apr 2010; accepted 21 Apr 2010; published 5 May 2010

reported in Ref [37]. Note also that for our cavity it is possible to tune the SRI range in which the maximum sensitivity occurs by changing the order of the TFBG cladding modes involved in the cavity spectrum.

In the TFBGs cavity structure proposed in 2008 [36], the sensor functionality is based on the coupling between the core mode and the ghost mode, leading to limitations on the tilt angles. On the other hand, our configuration is based on the possibility to operate on the cladding modes of the desired order and thus with selectable sensitivity and measuring ranges when bending and SRI have to be detected. This allows to use the tilt angle to select the order of excited cladding modes in the band of interest. To be sensitive within the desired SRI range, instead, the configuration of Ref [36] needs to operate on the total cavity length and thus on the attenuation along the fiber probe. Moreover, by increasing the uniform FBGs bandwidth in our cavity, the number of cladding modes dips involved in the reflected spectrum grows up with consequent advantages in terms of SRI and bending sensitivities.

As regards the interrogation mechanism, instead, in the case of Ref [36] the sensor is interrogated in transmission and spectral monitoring is required because the detection is based on the monitoring of the interference fringes visibility in correspondence of the ghost mode spectrum. For our configuration, the interrogation mechanism is in reflection and is based on standard and well assessed wavelength shift monitoring versus temperature and strain and intensity based measurements versus SRI and bending.

Also, in Ref [36] the possibility to multiplex several sensors by WDM techniques is supposed, but correct windowing of the transmitted signal by each sensor is required – due to the presence of the Bragg resonance and several cladding modes dips in transmission. The spectrum reflected by our cavity, instead, presents only the Bragg resonance of the TFBG outside of the useful signal bandwidth. In addition, this is true only if a weakly TFBG is considered – as happens for the cavities investigated in the paper. If the tilt angle is high enough to suppress the TFBG Bragg resonance, instead, our cavity will automatically reflect an intrinsically wavelength gated signal, ready to be multiplexed by means of WDM technique without further windowing operations. Note also that in our configuration different uniform FBG mirrors operating at different optical wavelengths and acting on the same TFBG provide a valid solution for a multi sensitivity sensor where sensitivity and measuring range are different for each wavelength gated signal reflected by the multi-mirror cavity. It is only necessary to inscribe more than a single couple of uniform and accorded FBGs at both sides of the TFBG.

Finally, if the single reflector configuration presented in Ref [35] is considered – there the sensor operation relies on the detection of the wavelength gated signal provided by a unique double passage of the light beam along the TFBG region – it is arguable that further optimization of the sensor sensitivity is not possible since multi-pass operation is not allowed. In this work, it is proposed the concept of cavity enabling multi-pass operation through the structure and allowing optimization margins of the final sensitivity, especially if the cavity modes interfere also in the spectral regions where attenuation bands of the tilted grating are located. Obviously this sensitivity tailoring is possible if the cavity is well balanced, thus requiring a proper design of the mirrors reflectivity combined with a suitable depth of the attenuation bands exhibited by the TFBG included in the cavity. This means that, by a proper cavity design, further optimization of the sensitivity characteristics of the structure is possible. In particular, a comparison with the data reported in Ref [35] reveals a similar SRI resolution for the two structures. This is because the cavity parameters – in terms of uniform FBGs reflectivities and depth of the TFBG cladding modes dips involved in the cavity spectrum – do not allow multi-pass interferometric operations along the structure. An analysis about the optimization of the cavity parameters to maximize the SRI sensitivity is currently in progress.

Acknowledgment

C. Caucheteur is supported by the Fonds National de la Recherche Scientifique (F.R.S.-FNRS).

#124953 - $15.00 USD Received 2 Mar 2010; revised 16 Apr 2010; accepted 21 Apr 2010; published 5 May 2010